ACS APPLIED MATERIALS & INTERFACES

Research Article

www.acsami.org

SERS-Fluorescence Monitored Drug Release of a Redox-Responsive Nanocarrier Based on Graphene Oxide in Tumor Cells

Hui Chen, Zhuyuan Wang,* Shenfei Zong, Lei Wu, Peng Chen, Dan Zhu, Chunlei Wang, Shuhong Xu, and Yiping Cui*

Advanced Photonics Center, Southeast University, 2# Sipailou, Nanjing 210096, Jiangsu China

Supporting Information

ABSTRACT: A redox-responsive drug carrier based on nanoscale graphene oxide (NGO) loaded with Ag nanoparticles, whose intracellular release behavior can be investigated by SERS-fluorescence combined spectroscopy, is presented. In this demonstrated drug carrier, to make the carrier integrated with the redox responsive property, we utilized disulfide linkages to load drug molecules to the surfaces of NGO directly, which can be cleaved by glutathione (GSH). Covalent drug loading and GSH-responsive release strategy can reduce the influence of the surface diffusion barriers introduced by multifunctionalization. Interestingly, the intracellular real-time drug release dynamics can be monitored by the combined SERS-fluorescence signals of the drugs, while the distribution of the drug carrier can simultaneously be tracked by the intrinsic SERS signals of NGO in the whole process. Our results show that upon the internalization of doxorubicin (DOX)-loaded nanocarriers into living cells, DOX was efficiently released under a GSH regulated reducing environment. Because tumor cells generally exhibit a higher concentration of GSH than normal ones, this drug carrier should have potential in the field of tumor therapy.

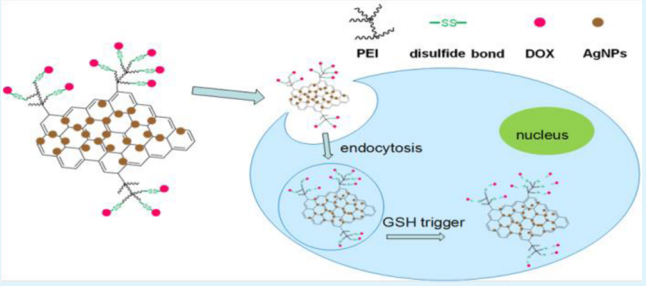

KEYWORDS: *graphene oxide, surface enhanced Raman scattering, stimuli−drug delivery, glutathione, tumor cells*

1. INTRODUCTION

Graphene oxide (GO) has been reported as a promising candidate in the field of drug carriers.[1−4] It is well-known that GO has several functional groups such as carboxyl, hydroxyl, and epoxy groups[5,6] that endow it with an aqueous solubility, a negative surface charge, and a capability to easily undergo further surface modifications.[7−9]

In biomedical applications, multifunctionalization has been chosen to modify the nanocarriers due to the particular biological requirements.[4,10−12] In previous reports on GO-based nanocarriers, drug molecules were usually loaded onto the GO sheets through $\pi-\pi$ stacking, which requires drug alternatives of aromatic molecules.[3,13] In addition, GO-based nanocarriers have often been functionalized with polymers, nanoparticles, or quantum dots to obtain the integrated properties, which will adversely affect the loading and release of drug molecules due to the surface diffusion barriers.[14] Therefore, it is important to address these critical issues on surface functionalization for the effective drug delivery. Considering this, covalently attaching drug molecules to nanoscale graphene oxide (NGO) can be of a choice to solve this problem, which no longer requires an aromatic domain. Thus, a triggering property can be integrated to make drug release respond to a specific kind of stimulus, such as the reducing environment of cancer sites.

Due to the sharp concentration difference of glutathione (GSH) between inside and outside cells, the disulfide bond will be cleaved only in the presence of GSH inside cells while being stable otherwise, which is promising in a controlled drug delivery system.[15] It is well-known that the high intracellular GSH level can reach to 10 mM while only approximately 2 μM for GSH outside cells.[16] The cytoplasmic GSH level in some kinds of cancer cells has been reported to be much higher than that in normal cells, which make it as an excellent stimulus for controlled drug delivery.[15,17,18]

For tracking the intracellular drug release dynamics, the dynamic information on the nanocarriers and drug are usually required simultaneously. Until now, the fluorescence technique has been widely employed by labeling the nanocarriers with dyes or quantum dots.[19] However, the fluorescence traceable nanocarriers might experience some undesirable problems. For instance, the fluorescence of the nanocarriers is easy to overlap with that of the drug due to the relatively wide bandwidth. Besides, the labeled dyes may leak out, which results in mistakes in tracing the nanocarriers precisely. This shows more limitations, especially when multiplex drug are used. Moreover, the problem of the leakage of the labeled dyes may not be easily solved unless the intrinsic signals of nanocarriers can be detected. Recently, surface enhanced Raman scattering (SERS), another powerful spectral technique, has attracted researchers

Received: May 14, 2014
Accepted: October 1, 2014
Published: October 1, 2014

Scheme 1. (A) Intracellular Drug Delivery of Redox-Reponsive DOX-Loaded NGO-Ag and (B) Synthesis Pathway of Disulfide-Based Drug Delivery System

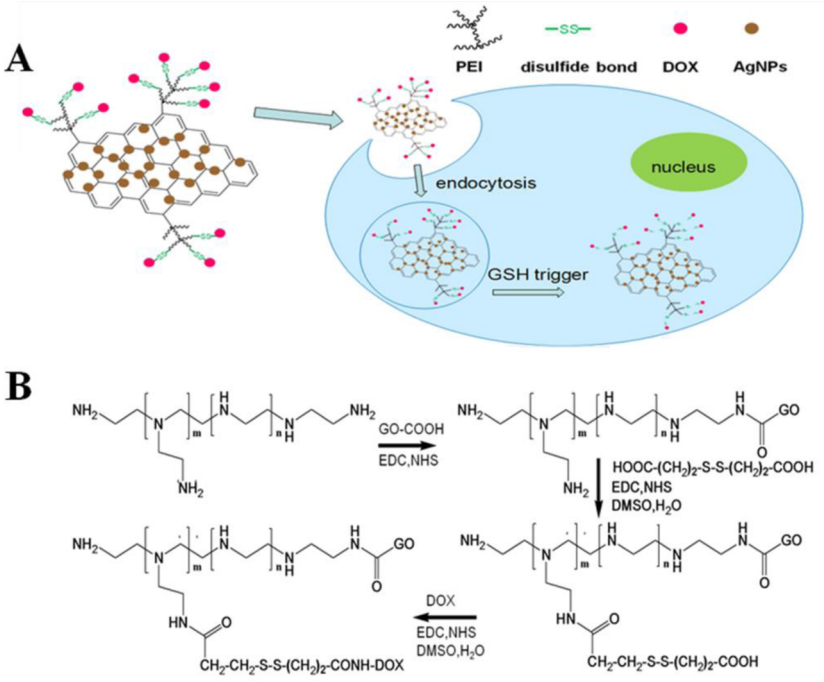

due to its advantages such as narrow spectral bands and abundant fingerprinting information.[20,21] A variety of SERS tags were applied in bioanalysis that show ultrasensitivity and quantitative abilities[22] such as sensing bacterial and antibacterial response[23] or monitoring drug release behaviors.[24,25] Previously, we have used the label-free SERS technique to track multiplex drugs and their dynamics in living cells,[26] which indicates that SERS is powerful enough to obtain dynamic and conformational information on drugs in living cells. However, SERS technique depends on a SERS-active substrate, which cannot be applied once the analyst is away from the substrate. Thus, combined SERS-fluorescence spectroscopy[27−29] is a powerful technique for monitoring the whole dynamic release process of nanocarriers and drugs in living cells.

Here, a redox-responsive drug carrier was demonstrated using an NGO-Ag nanocomposite, whose intracellular release behavior could be investigated by SERS-fluorescence combined signals. Scheme 1A illustrates the underlying mechanism of the nanocarrier design. The chemical structure and reaction conditions are shown in Scheme 1B. In such a nanocarrier, Ag nanoparticles are attached on the surfaces of NGO via an in situ reduction process that enhances the intrinsic Raman signals of NGO and drug molecules. Specifically, a straightforward method was designed to load drug molecules. Doxorubicin (DOX) was linked directly to the nanocarriers via disulfide bonds, which can be triggered by the intracellular GSH level. Importantly, through both the SERS and fluorescence signals of DOX, the dynamic release process of DOX from NGO inside living cells was investigated. Moreover, the distribution of intracellular nanocarriers can be tracked by detecting SERS signals of NGO without extra SERS reporters.

2. EXPERIMENTAL SECTION

2.1. Materials. Graphite powder and H_2O_2 (30%) were purchased from Sinopharm Chemical Reagent Co., Ltd. Silver nitrate ($AgNO_3$), poly(vinylpyrrolidone) (PVP; M_w, 30 000−40 000), *N*-hydroxysuccinimide (NHS), 1-ethyl-3-(3-(dimethylamino)propyl) carbodiimide (EDC), 3,3-dithiodipropionic acid (DTPA), polyethylenimine (PEI, 25 kDa), and dimethyl sulfoxide (DMSO) were purchased from Sigma-Aldrich. Phosphate buffered saline (PBS; pH, 7.4) was purchased from Beijing Biosynthesis Biotechnology Co., Ltd. Glutathione (GSH) and doxorubicin (DOX) were purchased from Aladdin Reagent Co., Ltd. Deionized water with a resistivity of 18.2 MΩ/cm was used in the experiments.

2.2. Nanoscale Graphene Oxide (NGO) Synthesis. Graphite oxide was synthesized by a modified Hummer's method.[30] In a typical experiment, 1 g of graphite powder was added into 23 mL of H_2SO_4 (98%), and the mixture was stirred for 12 h. Afterward, 4 g of $KMnO_4$ was added, the temperature was kept at less than 20 °C. The mixture was first stirred for 1 h and then stirred for 30 min at 40 °C. Next, the mixture was incubated in 100 °C for 30 min, then diluted to 100 mL with deionized water, and kept stirring for another 30 min. Subsequently, 10 mL of 30% H_2O_2 solution was added. For purification, the resulting mixture was washed with HCl solution (5%) and distilled water several times until the solution became neutral. The mixture was first exfoliated with an ultrasonic probe for 30 min at 400 W and then centrifugated at 10 000 rpm for 30 min. The supernatant was obtained to collect GO. The obtained GO was treated with an ultrasonic probe repeatedly at 520 W for 2 h, and finally, NGO was obtained. The obtained NGO was dispersed and stable in water for several months.

2.3. PEI Functionalized NGO (NGO-PEI). To modify the NGO surfaces with PEI, 2 mL of PEI aqueous solution (10% w/w) was added into 8 mL of NGO solution in the presence of EDC and NHS, followed by stirring for 2 h. Then, NGO-PEI was obtained by a centrifugation at 18 500 rpm for 20 min.

2.4. DOX-Conjugated NGO-PEI (DOX-SS-NGO). DOX was loaded to the NGO-PEI via disulfide bonds. Typically, 10 mL of DMSO solution containing 200 mg of EDC and 100 mg of NHS was stirred, followed by adding 50 mg of the DTPA. After 30 min, 8 mL of NGO-PEI solution was added, and the mixture was stirred for 24 h. The excess chemicals were removed through centrifugation. The obtained precipitate was dispersed in buffer solution with pH 5.3. Finally, 500 μL of DOX aqueous solution (10 mg/mL) was added and stirred overnight. The excess DOX was removed by centrifugation.

Finally, the product was redispersed into 10 mL of water. Thus, the DOX-SS-NGO was obtained.

2.5. In Situ Reduction (DOX-SS-NGO-Ag). Typically, 0.94 g of PVP was added to 8 mL of DOX-SS-NGO aqueous solution under stirring. Then, the mixture solution was heated to 60 °C and 1.5 mL of 188 mM $AgNO_3$ aqueous solution was added at the meanwhile and stirred completely for 5 min. Next, the mixture was incubated at 60 °C without agitation for 48 h. The resultant products were acquired by centrifugation (8000 rpm, 20 min). The precipitate was dispersed in 8 mL of water.

2.6. Instruments. Transmission electron microscope (TEM) images were acquired by a Tecnai G^2T20 electron microscope operating at 200 kV. The extinction spectra were measured using a Shimadzu UV-3600 PC spectrophotometer with quartz cuvettes of 1 cm optical path length. Fluorescence spectra were recorded by an Edinburgh FLS920 spectrometer. Intracellular fluorescence and SERS images were measured by an Olympus FV1000 microscopy at 488 and 633 nm excitation, respectively. The power of excitation light at 633 nm was about 2.3 mW at the sample. A holographic notch filter was employed to reduce the Rayleigh scattering light. The Raman signal was directed to an Andor shamrock spectrograph equipped with a charge-coupled device (CCD)

3. RESULTS AND DISCUSSION

3.1. Characterization of the Delivery System. To obtain the NGO, GO prepared by a modified Hummer's method[30] was cracked by an ultrasonic probe. Figure 2A shows the extinction spectrum of NGO. The peak of 230 nm, attributed to the π-plasmon of carbon,[31,32] remains essentially unchanged. Then, to modify the NGO surfaces with amino groups, a cationic branched polymer polyethylenimine (PEI) was conjugated to NGO sheets to modify the NGO, which can impart the stability in all biological solutions (Figure S4, Supporting Information) and attach DTPA through the formation of amide bonds. Conjugation of PEI was confirmed by XPS analysis (Figure S5, Supporting Information). EDC was utilized to activate carboxyl and promote the formation of amide bonds between DTPA and PEI by forming active mediates following stabilization by added NHS. In whole, DTPA was first attached to the amino groups on NGO surfaces. Next, DOX was conjugated to the attached DTPA through the formation of amide bonds between carboxyl of DTPA and amino of DOX. Thereby, DOX molecules were linked through disulfide bonds of DTPA (denoted as DOX-SS-NGO). The absorption spectrum of the DOX loaded NGO is shown in Figure 2A. A band at 488 nm attributed to DOX in the spectrum is observed, which confirms the loading of DOX onto NGO. It is noteworthy that in the process of DOX loading, DOX is expected to be loaded on the NGO through disulfide rather than $\pi-\pi$ stacking. So, DOX loading step was performed in buffer solution with pH 5.3, which can largely reduce the possibility of DOX directly adsorbed on NGO through $\pi-\pi$ stacking. The structure formed is evidenced by FTIR (Figure S2, Supporting Information) and better proves that DOX is chemically conjugated to the PEI-grafted NGO via a disulfide bond.

Finally, Ag NPs were attached onto DOX-SS-NGO through an in situ reduction process.[33,34] The morphology of the obtained DOX-SS-NGO-Ag was investigated. TEM images with different magnifications of DOX-SS-NGO-Ag are shown in Figure 1. The sizes of NGO were observed to be distributed from 100 to 400 nm with a relatively large range. The attached Ag NPs on the surfaces of NGO were also observed to be irregular. The average size is about 15 nm, as indicated by the TEM image with a higher magnification shown in Figure 1B.

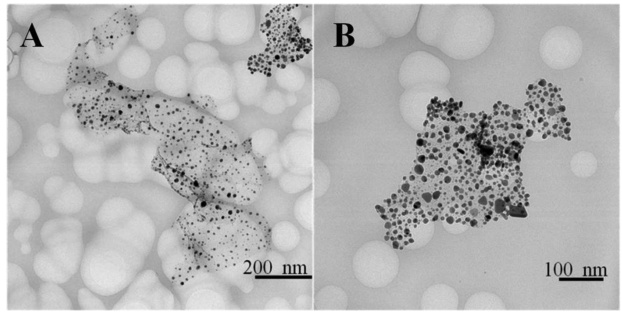

Figure 1. TEM images of DOX-SS-NGO-Ag with (A) low magnification and (B) high magnification.

The extinction spectrum is shown in Figure 2A. It is observed that a relatively broad band from 400 to 500 nm appears, which

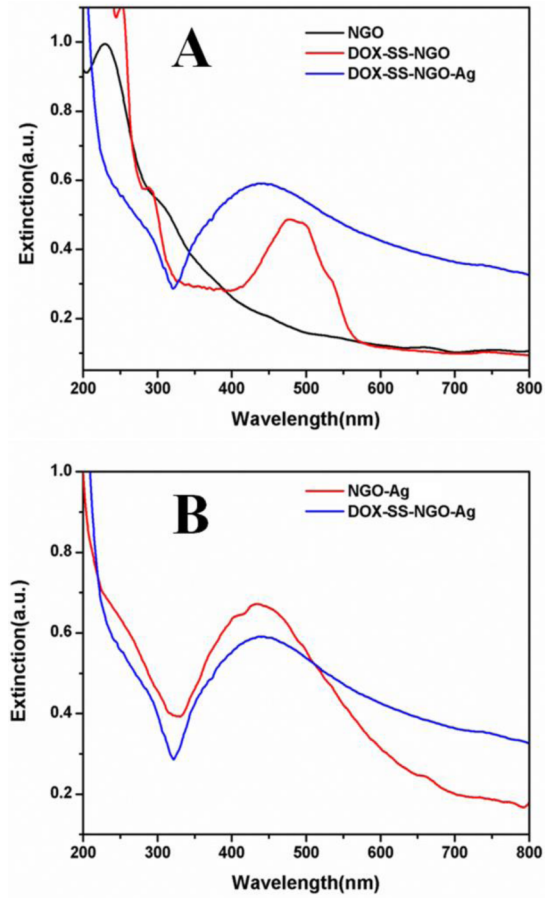

Figure 2. (A) Absorption spectra of the NGO, DOX-SS-NGO, and DOX-SS-NGO-Ag. (B) Absorption spectra of the NGO-Ag and DOX-SS-NGO-Ag.

is attributed to silver nanoparticles and DOX molecules. The characteristic peak of Ag NPs is located at about 430 nm, indicating the loading of Ag NPs onto the NGO sheets. The attached Ag NPs integrated with primary DOX resulted in a blue-shift in the curve as compared to the DOX-SS-NGO curve. The NGO-based carriers exhibited excellent stability and solubility in both of PBS (pH 7.4) and culture medium DMEM with 10% FBS (Figure S3A–C, Supporting Information). For a better comparison, the spectrum of Ag NPs attached on the surfaces of NGO without DOX is also measured (Figure 2B).

In the spectrum of DOX-SS-NGO-Ag, an obviously broader band around 500 nm is observed, which is associated with linked DOX molecules. Loading capacity was calculated to be 2.535 mg/mg in a 3:1 ratio of DOX to NGO-Ag.

3.2. SERS and Fluorescence Performance. The nanocarrier is designed to generate SERS signals of NGO itself by depositing Ag NPs on NGO surfaces. Thus, the locations of the intracellular nanocarrier can be tracked by the intrinsic SERS signals of NGO without extra SERS reporters. In addition, the optimal Raman enhancement of NGO can be obtained by tuning a ratio of $AgNO_3$ and NGO.[35] As shown in Figure 3A,

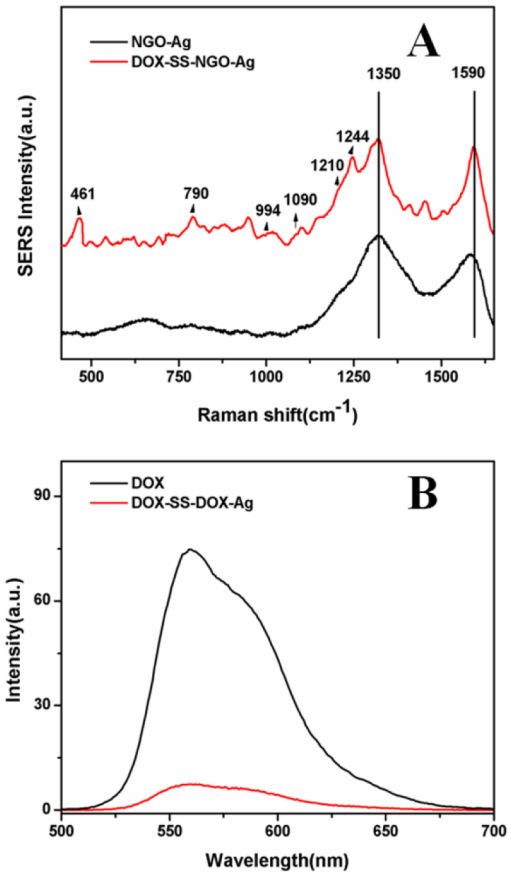

Figure 3. (A) SERS spectra of NGO-Ag and DOX-SS-NGO-Ag. (B) Photoluminescence spectra of free DOX and DOX-SS-NGO-Ag.

the SERS signals of NGO are remarkably enhanced by Ag NPs. Two intrinsic peaks at 1350 and 1590 cm^{-1} attributed to the D band and G band of NGO (corresponding to the symmetry A_{1g} and E_{2g} modes of sp^2 carbon atoms[36,37]) can be observed in the SERS spectrum of NGO-Ag.

Conjugation of DOX with NGO-Ag composite via disulfide also could be proved by the SERS spectra in Figure 3A. Compared with the SERS spectrum of NGO-Ag, it can be found that some new SERS peaks at 461, 790, 994, 1090, 1210, and 1244 cm^{-1} appear in the SERS spectrum of DOX-SS-NGO-Ag, which are associated with DOX.[38−40] In addition, fluorescence of DOX is drastically quenched by both of NGO and silver nanoparticles due to the energy transfer between DOX and NGO-Ag.[41−43] Figure 3B shows the fluorescence of both DOX−SS-NGO-Ag and free DOX with an equivalent concentration of DOX calculated from the DOX absorbance at 488 nm. Comparing the two spectra, it is obvious that the fluorescence of DOX was greatly reduced on NGO-Ag sheets, which provides further proof of the successful loading of DOX on NGO-Ag surfaces. Therefore, during the release process, the release behavior of DOX from NGO can be observed by using SERS signals of DOX. After DOX was detached from NGO, SERS signals of DOX disappeared, and the fluorescence of DOX was recovered to track the distribution inside living cells. However, SERS signals of NGO itself can still be utilized to track the distribution of nanocarriers before and after DOX release because Raman peaks of DOX have little influence on the SERS footprint of NGO.

3.3. Extracellular Drug Release Characteristics. The nanocarrier is designed for controlled intracellular drug delivery. Therefore, a triggering mechanism should be identified so that the loaded drug can be released upon a specific stimulus. In our presented nanocarriers, DOX is attached on NGO through a disulfide bond, which is responsive to a redox reducing environment. As is well-known, the in vivo redox reducing environment is modulated by glutathione (GSH).[44] Besides, the cytoplasmic GSH level in some kinds of tumor cells is found to be much higher than that in normal cells.[15] Thus, GSH with the high-level intracellular concentration is chosen as an excellent stimulus for controllable drug release, especially for tumor cells such as HeLa cells.[17,18] As reported previously, glutathione can also trigger the release of DOX loaded on graphene through $\pi-\pi$ stacking.[45] However, it seems the GSH sensitivity is not high enough because an external GSH treatment was needed, whereas our disulfide-based drug release system shows a much higher sensitivity of GSH because no additional treatment of external GSH in vitro is needed, and the intrinsic GSH level of tumor cells is enough to trigger the release.

After the nanocarriers were taken up by tumor cells upon to GSH, the disulfide linkage will be cleaved, and the DOX molecules were correspondingly released inside cells. Otherwise, the disulfide bonds maintain the stability outside the cells. Therefore, DOX molecules can be released from the surfaces of NGO only when the nanocarriers have entered tumor cells upon GSH. This presented delivery system is capable of avoiding the premature release of DOX. The release behavior of DOX can be well investigated via the absorbance, SERS, and fluorescence of DOX. To prove whether such nanocarriers are redox-responsive or not, GSH, which has the ability to cleave disulfide bonds, was used as the stimulus. In the experiments, DOX-SS-NGO-Ag was subjected to be dialyzed at 37 °C against GSH solutions with different concentrations. Then, the release process was studied at certain time durations within 24 h by investigating the fluorescence and absorbance of the dialysates. Figure 4A shows the time-dependent release characteristics of DOX at a given GSH level with different pH values. Under an environment without GSH at pH 5.3 or 7.4, the release amount of DOX was less than 10% within a time interval of 24 h. The slight increase of the releasing amount at pH 5.3 is caused by some noncovalently adsorbed DOX molecules. As reported by others, an obvious difference of DOX release amount existed between these two pH values when DOX was noncovalently adsorbed on NGO through $\pi-\pi$ stacking or hydrophobic interactions.[4,46] Thus, it could be deduced that in our nanocarriers, DOX molecules were mostly attached on NGO through disulfide bonds rather than noncovalent interactions. Moreover, it should be noted that the chosen pH values and GSH concentrations simulate the extracellular and intracellular environments. On the contrary,

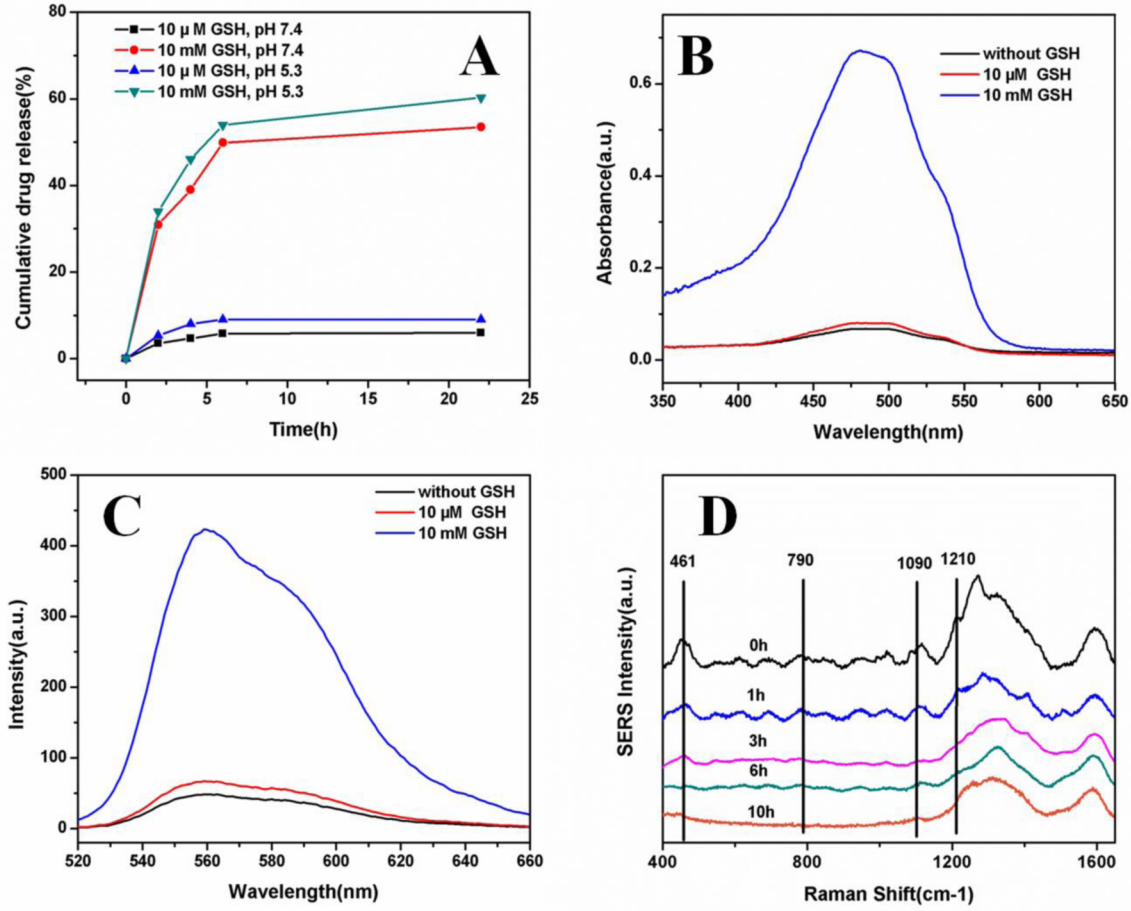

Figure 4. (A) GSH-mediated drug release curves of the nanocarriers at pH 7.4 and 5.3. (B) Absorbance and (C) fluorescence of the released DOX after DOX-SS-NGO-Ag was dialyzed for 24 h against different GSH concentrations. (D) Average SERS spectra of DOX-SS-NGO-Ag solution after being dialyzed for different time periods (n = 10).

once the nanocarriers were exposed to 10 mM GSH, the same as a typical cytoplasmic concentration of the tumor cells, about 60% of DOX was released in 24 h at pH 5.3. This releasing amount is much more than that in the presence of 10 μM GSH, which indicates a stimuli-responsive drug release ability. The drug release profile in 10% FBS solution was also conducted (Figure S3D, Supporting Information) which showed excellent GSH triggered drug release ability in serum. Besides, the experimental results obtained at pH 7.4 with 10 mM GSH also showed a rapid release of DOX, and the amount of released DOX is slightly less compared to pH 5.3, which may due to some noncovalent adsorbed DOX. Compared to the $\pi-\pi$ surface loading delivery system (Table S3 and Figure S7, Supporting Information), much higher loading and release efficiency of the disulfide-based system was obtained. This presented disulfide-based system can solve the surface diffusion barrier problem to some extent.

Figure 4B shows the absorbance of the released DOX after 24 h against different GSH concentrations, and the characteristic peak is at about 488 nm. It can be found that DOX was rapidly released with 10 mM GSH. However, GSH with a concentration of less than 10 μM was not abundant to trigger the observable DOX release. The fluorescence curves of the released DOX shown in Figure 4C also indicate the same results. For more accurate results, we investigated the SERS signals during the release process. As shown in Figure 4D, average SERS spectra of DOX-SS-NGO-Ag solution after being dialyzed for different time periods were detected. Raman peaks at 461, 790, 1090, and 1210 cm^{-1} attributed to DOX were utilized to monitor DOX release dynamics from NGO. SERS signals of DOX decreased obviously in the first 6 h and after this the signals were stable, which shows that DOX release was almost complete in the first 6 h. All of the above experimental results demonstrate that our presented nanocarriers can be used for a redox-responsive drug release. Meanwhile, the release dynamics can be monitored by SERS and fluorescence combined spectroscopy.

3.4. Intracellular Drug Delivery Characteristics. GSH-triggered drug release process was studied using HeLa cells as a model of tumor cells with a high GSH level. In the presented nanocarriers, the intrinsic Raman bands of NGO were enhanced by attaching Ag nanoparticles on the NGO surfaces, which were used to do SERS mapping images to express the distribution of nanocarriers inside HeLa cells. In addition, the real-time release dynamics were given by detection of SERS signals of DOX in situ inside HeLa cells. After the DOX was detached from NGO, SERS signals of DOX disappeared, and the recovered fluorescence signals of DOX were used to create fluorescence images to monitor its intracellular distribution. As reported previously, the nanocarriers were inside lysosomes for incubation with cells.[47] Here, we investigated the long-term intracellular effects (movements and distribution) of the nanocarriers. CLSM results of HeLa cells treated with DOX-loaded nanocarriers for different time intervals are shown in

Figure 5A–L, which clearly indicate of the intracellular DOX release process stimulated by GSH. As shown in Figure 5A–D,

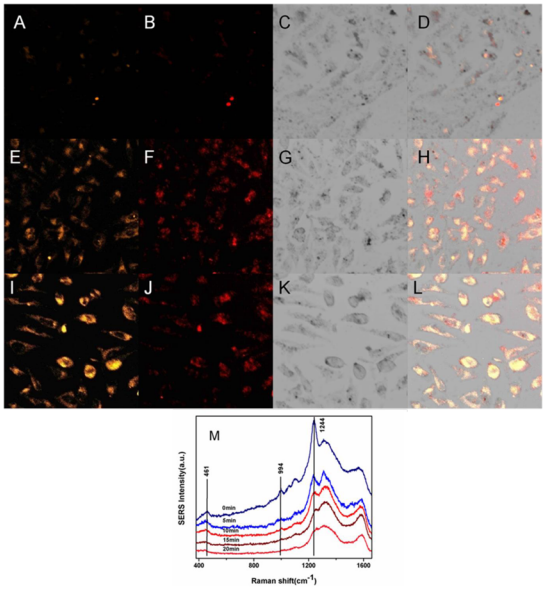

Figure 5. (A–L) Fluorescence, SERS, bright-field, and merged images of HeLa cells cultured with the drug delivery system for (A–D) 2 h, (E–H) 4 h, and (I–L) 8 h. (A, E, and I) Fluorescence images; (B, F, and J) SERS images; (C, G, and K) bright-field images; and (D, H, and L) merged images. In the intracellular experiments, SERS mapping image was produced by the 1590 cm^{-1} Raman band of NGO and fluorescence image was produced by fluorescence of DOX from 540 to 600 nm. (M) Average SERS spectra acquired from HeLa cells at different times after incubation for 4 h (n = 10).

when the HeLa cells were incubated with DOX loaded nanocarriers for 2 h, both the detected fluorescence and SERS signals were very weak, which indicated that the nanocarriers have not entered the cells and DOX was not released outside the cells. After 4 h of incubation (Figure 5E–H), the SERS mapping results showed that nanocarriers have been internalized in HeLa cells, which was accompanied by strong fluorescence in cells. This result shows that after the nanocarriers entered the cells, the intracellular GSH initiated a disulfide cleavage of DOX from the nanocarriers, triggering the efficient and controlled release of loaded DOX. For more accurate results of drug release from NGO-Ag surface, HeLa cells were incubated with DOX loaded nanocarriers for 4 h, and washed several times with PBS followed by recording the SERS spectra every 5 min. As shown in Figure 5M, the average SERS spectra obtained from HeLa cells show that the SERS intensity of bands (461, 994, and 1244 cm^{-1}) assigned to DOX decreased gradually within 20 min, and no SERS signals of DOX were observed after 20 min. Meanwhile, SERS intensity of bands 1350 and 1590 cm^{-1} assigned to GO was relatively stable in this progress. This means that the amount of loaded DOX decreased by release from the GO-Ag surface, which give us more accurate real-time drug release dynamics. In addition, SERS signals attributed to NGO were mainly observed in the lysosomes of HeLa cells while fluorescence was found in the cytoplasm region, which indicated that DOX have detached from the nanocarrriers (Figure 5H). After the nanocarriers were incubated with the cells for an even longer time (8 h, as shown in Figure 5I–L), fluorescence became still stronger in the cellular cytoplasm regions; meanwhile, the SERS signals were not observed to be increased obviously. However, the intracellular location of the nanocarriers was found not only in the lysosomes but also in the cytoplasm (Figure 5J), which is mainly due to the transporting motion of nanocarriers inside the cells. (Some of the nanocarriers escaped from the lysosome and were located in the cytoplasm, as shown in Figure S1, Supporting Information.) During this period, HeLa cells no longer took up more nanocarriers, reflected by the nearly stable SERS signals inside the cells. However, from the fluorescence images, it was found that the nanocarriers internalized in cells continuously released DOX. Consistent with the CLSM results, flow cytometry analysis also indicates the internalization of DOX-loaded nanocarriers (Figure S6, Supporting Information). Consequently, the specially engineered nanocarriers are capable of delivering the loaded drug to the environment with a high GSH level, such as the tumor sites.

Further, an MTT assay was used to quantify the cell viability of HeLa cells and evaluate the therapeutic efficacy of DOX-loaded nanocarriers. As shown in Figure 6A, NGO-Ag without DOX did not show significant cytotoxicity to HeLa cells with a high concentration of 1.0 mg mL^{-1}. However, either free DOX or DOX-loaded NGO-Ag with an equivalent DOX dose (12.8 μg mL^{-1}) has effectively reduced the viability of HeLa cells. The efficacy of about 40% viability after 24 h was achieved due to the loaded DOX molecules on NGO-Ag. Free DOX resulted in less than 20% viability of HeLa cells than the DOX loaded nanocarriers, which is mainly due to the stimulus-triggered release mechanism because release of DOX is controlled and not likely to be complete. The IC50 values were determined as 6.79 μg mL^{-1} for free DOX and 10.62 μg mL^{-1} for DOX loaded nanocarriers (Figure 6C).

4. CONCLUSION

We have successfully presented a redox-responsive nanocarrier based on NGO for the controlled drug release inside cells. Intrinsic SERS signals of NGO were used to monitor the distribution of the intracellular nanocarriers. Through a combination of SERS and fluorescence spectroscopy, the dynamic release characteristics of DOX from NGO inside living cells were investigated. When the cells were cultured for a short time (2 h), intracellular SERS signals of NGO or fluorescence signals of DOX were not observed, which confirmed that nanocarriers were not internalized by cells. After an incubation time of 4 h, the SERS and fluorescence signals with related to NGO and DOX were observed in different intracellular locations due to the drug molecules released from NGO upon exposure to intracellular reducing agent. More accurately, the real-time measurements of the SERS signals of DOX in living cells were utilized to track the release dynamics. All the results confirmed that the nanocarriers were capable of preferentially delivering the drug into a GSH reducing environment such as tumor sites. The in vitro experiments proved that such combined SERS–fluorescence spectroscopy is more powerful to track the drug release dynamics. Thus, this developed drug delivery system integrated with stimulus-triggered and optically tracked properties is promising in studying the interaction mechanism between nanomaterials and cells and in improving the therapeutic efficiency of tumor.

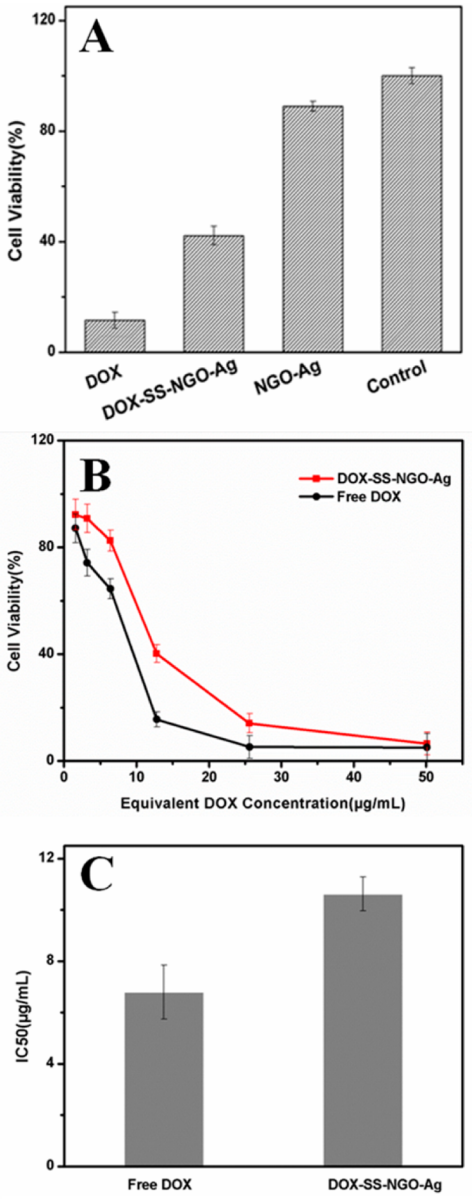

Figure 6. (A) Viability of HeLa cells cultured with free DOX, DOX-SS-NGO-Ag, and NGO-Ag. HeLa cells cultured with standard culture media were used as a control. (B) Viability of HeLa cells cultured with DOX loaded nanocarriers and free DOX with different concentrations. The equivalent DOX concentrations were 1.6, 3.2, 6.4, 12.8, 25.6, and 50.12 μg mL^{-1}, respectively. (C) IC50 values of DOX loaded nanocarriers and free DOX for HeLa cells.

■ ASSOCIATED CONTENT

Ⓢ Supporting Information

Figures S1−S8 and Tables S1−S3 exhibit the intensive study of the drug delivery system. This material is available free of charge via the Internet at http://pubs.acs.org.

■ AUTHOR INFORMATION

Corresponding Authors

*E-mail: cyp@seu.edu.cn. Fax: 86-25-83790201. Tel: 86-25-83792470.

*E-mail: wangzy@seu.edu.cn.

Notes

The authors declare no competing financial interest.

■ ACKNOWLEDGMENTS

This work was supported by the National Key Basic Research Programe of China (grant no. 2015CB352002), the National Natural Science Foundation of China (NSFC) (Nos. 60708024, 60877024, 61177033, and 21104009), the National Science Foundation for Excellent Young Scholars of Southeast University, xcellent Youth Foundation of Jiangsu Province (BK20140023), the Scientific Research Foundation of Graduate School of Southeast University (YBJJ1125), the Specialized Research Fund for the Doctoral Program of Higher Education (SRFDP) (Nos. 20070286058 and 20090092110015), and the Fundamental Research Funds for the Central Universities.

■ REFERENCES

(1) Bao, H. Q.; Pan, Y. Z.; Ping, Y.; Sahoo, N. G.; Wu, T. F.; Li, L.; Li, J.; Gan, L. H. Chitosan-Functionalized Graphene Oxide as a Nanocarrier for Drug and Gene Delivery. *Small* **2011**, *7*, 1569−1578.

(2) Liu, Z.; Robinson, J. T.; Sun, X. M.; Dai, H. J. PEGylated Nanographene Oxide for Delivery of Water-Insoluble Cancer Drugs. *J. Am. Chem. Soc.* **2008**, *130*, 10876−10877.

(3) Zhang, L. M.; Lu, Z. X.; Zhao, Q. H.; Huang, J.; Shen, H.; Zhang, Z. J. Enhanced Chemotherapy Efficacy by Sequential Delivery of siRNA and Anticancer Drugs Using PEI-Grafted Graphene Oxide. *Small* **2011**, *7*, 460−464.

(4) Zhang, L. M.; Xia, J. G.; Zhao, Q. H.; Liu, L. W.; Zhang, Z. J. Functional Graphene Oxide as a Nanocarrier for Controlled Loading and Targeted Delivery of Mixed Anticancer Drugs. *Small* **2010**, *6*, 537−544.

(5) Yuge, R.; Zhang, M. F.; Tomonari, M.; Yoshitake, T.; Iijima, S.; Yudasaka, M. Site Identification of Carboxyl Groups on Graphene Edges with Pt Derivatives. *ACS Nano* **2008**, *2*, 1865−1870.

(6) Langley, L. A.; Villanueva, D. E.; Fairbrother, D. H. Quantification of Surface Oxides on Carbonaceous Materials. *Chem. Mater.* **2006**, *18*, 169−178.

(7) Park, S.; Ruoff, R. S. Chemical Methods for the Production of Graphenes. *Nat. Nanotechnol.* **2009**, *4*, 217−224.

(8) Szabo, T.; Berkesi, O.; Forgo, P.; Josepovits, K.; Sanakis, Y.; Petridis, D.; Dekany, I. Evolution of Surface Functional Groups in a Series of Progressively Oxidized Graphite Oxides. *Chem. Mater.* **2006**, *18*, 2740−2749.

(9) Chen, C.; Cai, W. M.; Long, M. C.; Zhou, B. X.; Wu, Y. H.; Wu, D. Y.; Feng, Y. J. Synthesis of Visible-Light Responsive Graphene Oxide/TiO_2 Composites with p/n Heterojunction. *ACS Nano* **2010**, *4*, 6425−6432.

(10) Fang, M.; Wang, K. G.; Lu, H. B.; Yang, Y. L.; Nutt, S. Covalent Polymer Functionalization of Graphene Nanosheets and Mechanical Properties of Composites. *J. Mater. Chem.* **2009**, *19*, 7098−7105.

(11) Sun, S. T.; Cao, Y. W.; Feng, J. C.; Wu, P. Y. Click Chemistry as a Route for the Immobilization of Well-Defined Polystyrene onto Graphene Sheets. *J. Mater. Chem.* **2010**, *20*, 5605−5607.

(12) Sun, S. T.; Wu, P. Y. A One-Step Strategy for Thermal- and pH-Responsive Graphene Oxide Interpenetrating Polymer Hydrogel Networks. *J. Mater. Chem.* **2011**, *21*, 4095−4097.

(13) Sun, X. M.; Liu, Z.; Welsher, K.; Robinson, J. T.; Goodwin, A.; Zaric, S.; Dai, H. J. Nano-Graphene Oxide for Cellular Imaging and Drug Delivery. *Nano Res.* **2008**, *1*, 203−212.

(14) Wen, H. Y.; Dong, C. Y.; Dong, H. Q.; Shen, A. J.; Xia, W. J.; Cai, X. J.; Song, Y. Y.; Li, X. Q.; Li, Y. Y.; Shi, D. L. Engineered Redox-Responsive PEG Detachment Mechanism in PEGylated Nano-Graphene Oxide for Intracellular Drug Delivery. *Small* **2012**, *8*, 760−769.

(15) Bauhuber, S.; Hozsa, C.; Breunig, M.; Gopferich, A. Delivery of Nucleic Acids via Disulfide-Based Carrier Systems. *Adv. Mater.* **2009**, *21*, 3286−3306.

(16) Meng, F. H.; Hennink, W. E.; Zhong, Z. Reduction-Sensitive Polymers and Bioconjugates for Biomedical Applications. *Biomaterials* **2009**, *30*, 2180−2198.

(17) Wen, H. Y.; Dong, H. Q.; Xie, W. J.; Li, Y. Y.; Wang, K.; Pauletti, G. M.; Shi, D. L. Rapidly Disassembling Nanomicelles with Disulfide-Linked PEG Shells for Glutathione-Mediated Intracellular Drug Delivery. *Chem. Commun.* **2011**, *47*, 3550−3552.
(18) Takae, S.; Miyata, K.; Oba, M.; Ishii, T.; Nishiyama, N.; Itaka, K.; Yamasaki, Y.; Koyama, H.; Kataoka, K. PEG-Detachable Polyplex Micelles based on Disulfide-Linked Block Catiomers as Bioresponsive Nonviral Gene Vectors. *J. Am. Chem. Soc.* **2008**, *130*, 6001−6009.
(19) Kang, B.; Li, J.; Chang, S. Q.; Dai, M. Z.; Ren, C.; Dai, Y. D.; Chen, D. Subcellular Tracking of Drug Release from Carbon Nanotube Vehicles in Living Cells. *Small* **2012**, *8*, 777−782.
(20) Niu, J. J.; Schrlau, M. G.; Friedman, G.; Gogotsi, Y. Carbon Nanotube-Tipped Endoscope for in Situ Intracellular Surface-Enhanced Raman Spectroscopy. *Small* **2011**, *7*, 540−545.
(21) Wang, Z. Y.; Zong, S. F.; Li, W.; Wang, C. L.; Xu, S. H.; Chen, H.; Cui, Y. P. SERS−Fluorescence Joint Spectral Encoding Using Organic−Metal−QD Hybrid Nanoparticles with a Huge Encoding Capacity for High-Throughput Biodetection: Putting Theory into Practice. *J. Am. Chem. Soc.* **2012**, *134*, 2993−3000.
(22) Wang, Y. Q.; Yan, B.; Chen, L. X. SERS Tags: Novel Optical Nanoprobes for Bioanalysis. *Chem. Rev.* **2013**, *113*, 1391−1428.
(23) Lin, D. H.; Qin, T. Q.; Wang, Y. Q.; Sun, X. Y.; Chen, L. X. Graphene Oxide Wrapped SERS Tags: Multifunctional Platforms toward Optical Labeling, Photothermal Ablation of Bacteria, and the Monitoring of Killing Effect. *ACS Appl. Mater. Interfaces* **2014**, *6*, 1320−1329.
(24) Ock, K.; Jeon, W. I.; Ganbold, E. O.; Kim, M.; Park, J.; Seo, J. H.; Cho, K.; Joo, S. W.; Lee, S. Y. Real-Time Monitoring of Glutathione-Triggered Thiopurine Anticancer Drug Release in Live Cells Investigated by Surface-Enhanced Raman Scattering. *Anal. Chem.* **2012**, *84*, 2172−2178.
(25) Tian, L. M.; Gandra, N.; Singamaneni, S. Monitoring Controlled Release of Payload from Gold Nanocages Using Surface Enhanced Raman Scattering. *ACS Nano* **2013**, *7*, 4252−4260.
(26) Yang, J.; Cui, Y. P.; Zong, S. F.; Zhang, R. H.; Song, C. Y.; Wang, Z. Y. Tracking Multiplex Drugs and Their Dynamics in Living Cells Using the Label-Free Surface-Enhanced Raman Scattering Technique. *Mol. Pharmaceutics* **2012**, *9*, 842−849.
(27) Kang, B.; Afifi, M. M.; Austin, L. A.; El-Sayed, M. A. Exploiting the Nanoparticle Plasmon Effect: Observing Drug Delivery Dynamics in Single Cells via Raman/Fluorescence Imaging Spectroscopy. *ACS Nano* **2013**, *7*, 7420−7427.
(28) Wang, Y. Q.; Chen, L. X.; Liu, P. Biocompatible Triplex Ag@SiO_2@mTiO_2 Core-Shell Nanoparticles for Simultaneous Fluorescence-SERS Bimodal Imaging and Drug Delivery. *Chem.—Eur. J.* **2012**, *18*, 5935−5943.
(29) Zong, S. F.; Wang, Z. Y.; Chen, H.; Yang, J.; Cui, Y. P. Surface Enhanced Raman Scattering Traceable and Glutathione Responsive Nanocarrier for the Intracellular Drug Delivery. *Anal. Chem.* **2013**, *85*, 2223−2230.
(30) Hummers, W. S.; Offeman, R. E. Preparation of Graphitic Oxide. *J. Am. Chem. Soc.* **1958**, *80*, 1339−1339.
(31) Reed, B. W.; Sarikaya, M. Electronic Properties of Carbon Nanotubes by Transmission Electron Energy-Loss Spectroscopy. *Phys. Rev. B: Condens. Matter Mater. Phys.* **2001**, *64*, 195404.
(32) Attal, S.; Thiruvengadathan, R.; Regev, O. Determination of the Concentration of Single-Walled Carbon Nanotubes in Aqueous Dispersions Using UV−Visible Absorption Spectroscopy. *Anal. Chem.* **2006**, *78*, 8098−8104.
(33) Zhang, Z.; Xu, F. G.; Yang, W. S.; Guo, M. Y.; Wang, X. D.; Zhanga, B. L.; Tang, J. L. A Facile One-Pot Method to High-Quality Ag-Graphene Composite Nanosheets for Efficient Surface-Enhanced Raman Scattering. *Chem. Commun.* **2011**, *47*, 6440−6442.
(34) Tang, X. Z.; Cao, Z. W.; Zhang, H. B.; Liu, J.; Yu, Z. Z. Growth of Silver Nanocrystals on Graphene by Simultaneous Reduction of Graphene Oxide and Silver Ions with a Rapid and Efficient One-Step Approach. *Chem. Commun.* **2011**, *47*, 3084−3086.
(35) Liu, Z. M.; Guo, Z. Y.; Zhong, H. Q.; Qin, X. C.; Wan, M. M.; Yang, B. W. Graphene Oxide based Surface-Enhanced Raman Scattering Probes for Cancer Cell Imaging. *Phys. Chem. Chem. Phys.* **2013**, *15*, 2961−2966.
(36) Ferrari, A. C.; Robertson, J. Interpretation of Raman Spectra of Disordered and Amorphous Carbon. *Phys. Rev. B: Condens. Matter Mater. Phys.* **2000**, *61*, 14095−14107.
(37) Kudin, K. N.; Ozbas, B.; Schniepp, H. C.; Prud'homme, R. K.; Aksay, I. A.; Car, R. Raman Spectra of Graphite Oxide and Functionalized Graphene Sheets. *Nano Lett.* **2008**, *8*, 36−41.
(38) Nabiev, I. R.; Morjani, H.; Manfait, M. Selective Analysis of Antitumor Drug-Interaction with Living Cancer-Cells as Probed by Surface-Enhanced Raman-Spectroscopy. *Eur. Biophys. J.* **1991**, *19*, 311−316.
(39) Sokolov, K.; Khodorchenko, P.; Petukhov, A.; Nabiev, I.; Chumanov, G.; Cotton, T. M. Contributions of Short-Range and Classical Electromagnetic Mechanisms to Surface-Enhanced Raman-Scattering from Several Types of Biomolecules Adsorbed on Cold-Deposited Island Films. *Appl. Spectrosc.* **1993**, *47*, 515−522.
(40) Yang, J.; Wang, Z. Y.; Zong, S. F.; Chen, H.; Zhang, R. H.; Cui, Y. P. Dual-Mode Tracking of Tumor-Cell-Specific Drug Delivery Using Fluorescence and Label-Free SERS Techniques. *Biosens. Bioelectron.* **2014**, *51*, 82−89.
(41) He, S. J.; Song, B.; Li, D.; Zhu, C. F.; Qi, W. P.; Wen, Y. Q.; Wang, L. H.; Song, S. P.; Fang, H. P.; Fan, C. H. A Graphene Nanoprobe for Rapid, Sensitive, and Multicolor Fluorescent DNA Analysis. *Adv. Funct. Mater.* **2010**, *20*, 453−459.
(42) Li, J.; Lu, C. H.; Yao, Q. H.; Zhang, X. L.; Liu, J. J.; Yang, H. H.; Chen, G. N. A Graphene Oxide Platform for Energy Transfer-based Detection of Protease Activity. *Biosens. Bioelectron.* **2011**, *26*, 3894−3899.
(43) Nabika, H.; Deki, S. Enhancing and Quenching Functions of Silver Nanoparticles on the Luminescent Properties of Europium Complex in the Solution Phase. *J. Phys. Chem. B* **2003**, *107*, 9161−9164.
(44) Ballatori, N.; Krance, S. M.; Notenboom, S.; Shi, S. J.; Tieu, K.; Hammond, C. L.; Hammond, C. L. Glutathione Dysregulation and the Etiology and Progression of Human Diseases. *Biol. Chem.* **2009**, *390*, 191−214.
(45) Dembereldorj, U.; Kim, M.; Kim, S.; Ganbold, E. O.; Lee, S. Y.; Joe, S. W. A Spatiotemporal Anticancer Drug Release Platform of PEGylated Graphene Oxide Triggered by Glutathione in Vitro and in Vivo. *J. Mater. Chem.* **2012**, *22*, 23845−23851.
(46) Yang, X. Y.; Zhang, X. Y.; Liu, Z. F.; Ma, Y. F.; Huang, Y.; Chen, Y. High-Efficiency Loading and Controlled Release of Doxorubicin Hydrochloride on Graphene Oxide. *J. Phys. Chem. C* **2008**, *112*, 17554−17558.
(47) Huang, J.; Zong, C.; Shen, H.; Cao, Y. H.; Ren, B.; Zhang, Z. J. Tracking the Intracellular Drug Release from Graphene Oxide Using Surface-Enhanced Raman Spectroscopy. *Nanoscale* **2013**, *5*, 10591−10598.